Acta Crystallographica Section D
Biological Crystallography
ISSN 0907-4449

A neutron crystallographic analysis of T_6 porcine insulin at 2.1 Å resolution

Wakari Iwai,[a] Taro Yamada,[b] Kazuo Kurihara,[c] Yuki Ohnishi,[d] Yoichiro Kobayashi,[a] Ichiro Tanaka,[d] Haruyuki Takahashi,[a] Ryota Kuroki,[c] Taro Tamada[c] and Nobuo Niimura[b]*

[a]Graduate School of Science and Engineering, Ibaraki University, Hitachi, Naka-Narusawa 4-12-1, Ibaraki 316-8511, Japan, [b]Frontier Research Center for Applied Atomic Sciences, Ibaraki University, Shirakata 162-1, Tokai, Ibaraki 319-1106, Japan, [c]Japan Atomic Energy Agency, Shirakata-shirane 2-4, Tokai, Ibaraki 319-1195, Japan, and [d]Faculty of Engineering, Ibaraki University, Hitachi, Naka-Narusawa 4-12-1, Ibaraki 316-8511, Japan

Correspondence e-mail: niimura@mx.ibaraki.ac.jp

Received 10 December 2008
Accepted 14 July 2009

PDB Reference: T_6 porcine insulin, 3fhp, r3fhpsf.

Neutron diffraction data for T_6 porcine insulin were collected to 2.1 Å resolution from a single crystal partly deuterated by exchange of mother liquor. A maximum-likelihood structure refinement was undertaken using the neutron data and the structure was refined to a residual of 0.179. The hydrogen-bonding network of the central core of the hexamer was observed and the charge balance between positively charged Zn ions and their surrounding structure was interpreted by considering the protonation and/or deprotonation states and interactions of HisB10, water and GluB13. The observed double conformation of GluB13 was essential to interpreting the charge balance and could be compared with the structure of a dried crystal of T_6 human insulin at 100 K. Differences in the dynamic behaviour of the water molecules coordinating the upper and lower Zn ions were observed and interpreted. The hydrogen bonds in the insulin molecules, as well as those involving HisB10 and GluB13, are discussed. The hydrogen/deuterium (H/D) exchange ratios of the amide H atoms of T_6 porcine insulin in crystals were obtained and showed that regions highly protected from H/D exchange are concentrated in the centre of a helical region of the B chains. From the viewpoint of soaking time *versus* H/D-exchange ratios, the amide H atoms can be classified into three categories.

1. Introduction

Insulin is a polypeptide hormone that is critical to the metabolism of glucose. The insulin monomer consists of two chains, a 21-residue A chain and a 30-residue B chain, linked by a pair of disulfide bonds, A7–B7 and A20–B19; furthermore, an additional intrachain disulfide bond links A6 and A11. The structure of hexameric insulin, which is the form in which it is stored in the pancreas, was first reported in 1969 (Adams *et al.*, 1969) and a comprehensive description of the room-temperature structure at 1.5 Å resolution, as well as the biological implications thereof, has been published (Baker *et al.*, 1988). The structure of the insulin monomer has been determined by NMR and the crystal structures of modified monomers and insulin-like growth factor (IGF) relevant to the active species have also been determined by X-ray analysis (Blundell *et al.*, 1971, 1972). The insulin hexamer is an allosteric protein that undergoes transitions between three allosteric forms (Brzovic *et al.*, 1994): T_6, T_3R_3 and R_6 (Kaarsholm *et al.*, 1990). In both the T_6 and R_6 states small conformational differences in the monomers of each dimer unit give rise to three pseudo-twofold symmetry axes.

In the case of the T_6 state, the crystal asymmetric unit contains two insulin monomers (a dimer) related by a pseudo-

© 2009 International Union of Crystallography
Printed in Singapore – all rights reserved

twofold axis; the crystallographic threefold axis generates the insulin hexamer from three dimers. Two zinc ions on opposite sides of the hexamer are situated on the crystallographic threefold axis; each is octahedrally coordinated by the three crystallographically related HisB10 $N^{\varepsilon 2}$ (N_τ) atoms and three water molecules.

To understand the octahedrally coordinated structure and the coordination mechanism thereof, it is essential to know the protonation and/or deprotonation states of not only HisB10 $N^{\varepsilon 2}$ but also HisB10 $N^{\delta 1}$ (N_π). Moreover, it is of interest to understand how the zinc positive charge is balanced by negatively charged glutamic acid carboxyl groups or other groups. The protonation and/or deprotonation states of polar amino-acid residues must be explored by neutron diffraction.

At the centre of the hexamer, the six GluB13 side-chain carboxylate groups form a hydrogen-bond network that spans the central cavity. Smith *et al.* (2003) suggested that a short strong centred carboxylate–carboxylic acid hydrogen bond links pairs of independent GluB13 carboxylate groups, with a proton shared equally between the pairs of partially charged OE2 atoms.

The joint neutron and X-ray structure of T_6 porcine insulin was initially determined at 2.2 Å resolution based on 6253 reflections that were measured and integrated using the dynamic mask procedure; this yielded 3142 independent reflections, of which 2253 were observed ($I > 1.5\sigma$; Wlodawer *et al.*, 1989). However, there was no evidence for protonation of GluB13 in the neutron density maps and Wlodawer and coworkers concluded that the existence of a hydrogen bond could not be confirmed; a nonbonded interaction was instead suggested.

We have carried out a neutron crystallographic analysis of T_6 porcine insulin at 2.1 Å resolution using 4824 independent reflections from 13 038 observed reflections. The charge balance surrounding the zinc ions, the time-evolution of the H/D-exchange rate and the protonation and deprotonation states of ionized amino-acid residues will be discussed. Moreover, porcine insulin can crystallize in a cubic space group without zinc and neutron crystallographic analyses of this cubic insulin at pD values of 6.6 and 9.0 have been carried out. This has enabled the protonation and/or deprotonation states to be clearly observed and the significance of the abnormal pK_a value of HisB10 to be revealed (Maeda *et al.*, 2004; Ishikawa, Chatake, Ohnishi *et al.*, 2008; Ishikawa, Chatake, Morimoto *et al.*, 2008). In the present study, the structure of T_6 porcine insulin will be compared with that of cubic insulin.

2. Material and methods

2.1. Crystallization

Porcine insulin was purchased from Sigma–Aldrich Co. (I-5523; St Louis, Missouri, USA). A rough crystallization-phase diagram for T_6 porcine insulin was determined using a batch method; a large single crystal was grown based on this crystallization-phase diagram as follows. A crystal starts growing in the nucleation region just above the nucleation borderline; as the crystal grows, the protein concentration decreases into the metastable region. Spontaneously, this crystal becomes the seed crystal and continues to grow in the metastable region. It is advantageous to grow a crystal in the metastable region because there is no further appearance of nucleation (Ohnishi *et al.*, 2009). In the present study, the final conditions for growing a large single crystal corresponded to concentrations of 2.3 mg ml^{-1} insulin, 50 m*M* sodium citrate, 6 m*M* zinc sulfate and 17% acetone at pH 6.3. The crystal grew to 2 mm^3 in volume after four weeks, which is a suitable size for a neutron diffraction experiment. Thereafter, the crystal was soaked in deuterated solution for one month in order to reduce background scattering from H atoms, which have a large incoherent neutron scattering length. Finally, the crystal was mounted in a sealed quartz capillary (3 mm diameter).

Table 1
Statistics pertaining to data collection, reduction and refinement.

Values in parentheses are for the outer shell of data (2.19–2.11 Å).

Data collection	
Space group	*R*3
Unit-cell parameters (Å)	$a = b = 82.85$, $c = 34.17$
Beam port/radiation	1G, JRR-3
Wavelength (Å)	2.6
Diffractometer	BIX-4
Temperature (K)	293
Exposure time (min per frame)	120
Total frames	487
Maximum resolution (Å)	2.11
Observed reflections	13038
Unique reflections	4824 (303)
Redundancy	2.7
Completeness ($I > -3\sigma$) (%)	90.5 (61.0)
$R_{\rm merge}$ (%)	14.2 (25.2)
Refinement	
Resolution (Å)	80–2.11 (2.19–2.11)
PDB code	3fhp
$R_{\rm cryst}$ (%)	17.9
$R_{\rm free}$ (%)	25.6
No. of non-H atoms	730
No. of H atoms	688
No. of D atoms	341
Ramachandran allowed regions (%)	93.0
Ramachandran additionally allowed regions (%)	5.8
Ramachandran generously allowed regions (%)	1.2
No. of DOD molecules	85
No. of water molecules (O form)	4

2.2. Data collection and refinement

T_6 porcine insulin crystallizes in the hexagonal space group *R*3, with unit-cell parameters $a = b = 82.85$, $c = 34.17$ Å. The neutron diffraction experiment was carried out at room temperature using a BIX-4 single-crystal diffractometer installed at the JRR-3 reactor of the Japan Atomic Energy Agency (Niimura *et al.*, 1994, 2006; Kurihara *et al.*, 2004). A stepwise scanning method with an interval of 0.3° was used to collect data; the exposure time was 120 min per frame. After collecting 207 frames, the crystal rotation axis was changed by about 90° to a different rotation axis, whereupon an additional 280 frames were collected. The reflection intensities were

integrated and scaled with *DENZO* and *SCALEPACK* (Otwinowski & Minor, 1997). Subsequent data reduction was performed using the *CCP*4 program *TRUNCATE* (Collaborative Computational Project, Number 4, 1994). A total of 4824 independent reflections were obtained with an overall $R_{\rm merge}$ of 14.2% from 13 038 observed reflections. The effective resolution was estimated as 2.1 Å from analysis of the amplitudes of the observed structure factors (Swanson, 1988). Refinement was carried out using the programs *CNS* (Brünger *et al.*, 1998) and *XtalView* (McRee, 1999). The X-ray structure of T_6 porcine insulin determined at 1.50 Å resolution (PDB code 4ins; Baker *et al.*, 1988) was used as an initial model. Firstly, putative non-exchangeable H atoms were placed into the initial model; the exchangeable H atoms were then found by carrying out an OMIT map for each amino-acid residue in turn. Secondly, a positional refinement of all the atoms was performed. Thereafter, D_2O molecules were added corresponding to peaks found in the $F_o - F_c$ map. The final model contained 89 water molecules (D_2O, 85; ball-shaped, 4). The $R_{\rm free}$ value was 25.6% (for 5% of reflections that were not used in the refinement) and the $R_{\rm cryst}$ value was 17.9% for all data to 2.1 Å resolution (Brünger, 1992). The statistics of data reduction and structure refinement are summarized in Table 1.

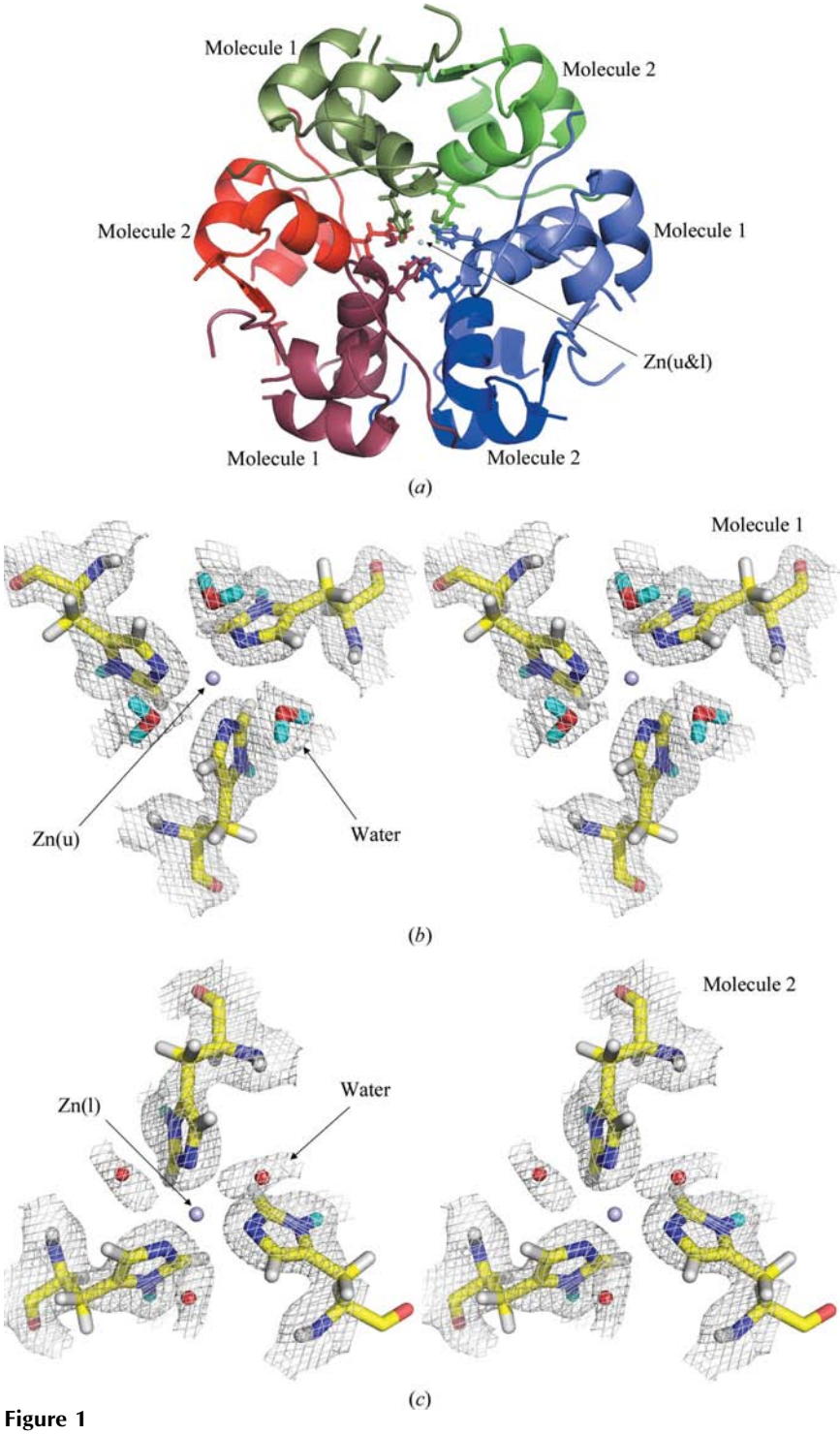

Figure 1
(*a*) Molecular structure of an insulin hexamer, as determined in the present neutron diffraction experiment, viewed down the threefold axis. The water molecules coordinating the Zn ions are shown in stereoviews (*b*) down the threefold axis to the upper Zn [Zn(u)] and (*c*) up the threefold axis to the lower Zn [Zn(l)]. The map is a $2|F_o| - |F_c|$ positive nuclear density map contoured at 1σ. The stereoviews were prepared with the *PyMOL* program (DeLano, 2002).

3. Results and discussion

3.1. Zinc coordination and hexamer formation

In an aqueous solution with a pH of 5–8, insulin aggregates in the presence of zinc ions to form a hexamer (Goldman & Carpenter, 1974) as shown in Fig. 1(*a*). In the T_6 insulin crystals, three dimers are assembled around two zinc ions (upper Zn and lower Zn) that are 16.4 Å apart on the threefold axis. Figs. 1(*b*) and 1(*c*) show $2F_o - F_c$ maps of the areas around the upper Zn and lower Zn, respectively. The $N^{\varepsilon 2}$ atom of HisB10 is deprotonated and coordinated to Zn, whereas $N^{\delta 1}$ of HisB10 is protonated, making the net charge of HisB10 neutral. The two molecules in the dimer are designated molecule 1 and molecule 2, as shown in Figs. 1(*b*) and 1(*c*), respectively. Residues belonging to molecule 1 or molecule 2 are distinguished by the suffix .1 or .2 after the residue number. Thus, the upper zinc is coordinated to three symmetry-related $N^{\varepsilon 2}$ atoms of HisB10.1 (*i.e.* from molecule 1) and three water molecules, while the lower Zn is coordinated to the three symmetry-related $N^{\varepsilon 2}$ atoms of HisB10.2 and three water molecules, as shown in Figs. 1(*b*) and 1(*c*), respectively. Three water molecules can be seen to coordinate the upper Zn from the

top (Fig. 1*b*) and another three water molecules can be seen to coordinate the lower Zn from the bottom (Fig. 1*c*). The former three water molecules were classified as triangular, since the D atoms of these water molecules could be placed. On the other hand, the latter three water molecules were classified as ball-shaped and are presumably freely rotating. These classifications are supported well by the *B* factors. The *B* factors of the triangular molecules are smaller (36.5 Å^2) than those of the ball-shaped molecules (74.0 Å^2) (Chatake *et al.*, 2003). Differences in the dynamic behaviour of the coordinated water molecules between the upper and lower Zn ions were also observed in the structure of T_6 human insulin at 1.0 Å resolution at 120 K (Smith *et al.*, 2003), in which the unambiguous electron density of three water molecules coordinating the upper Zn ion was observed. Continuous electron density for the three water molecules coordinating the lower Zn ion was also observed, suggesting that it would be possible for a disordered anion such as a citrate to occupy this site (Smith *et al.*, 2003). Furthermore, in the structure of a dried crystal of T_6 human insulin at 100 K (Smith & Blessing, 2003) the upper Zn ion bound three water molecules and adopted an octahedral coordination in the crystal, whereas the lower zinc ion adopted a tetrahedral coordination with the three water molecules being replaced by a single chloride ion.

In our neutron results, a difference in the temperature factor of $N^{\varepsilon 2}$ of HisB10 coordinating to the Zn ions was also observed. The temperature factors were 9.3 Å^2 for $N^{\varepsilon 2}$ of HisB10.1 coordinating to the upper Zn ion and 14.6 Å^2 for $N^{\varepsilon 2}$ of HisB10.2 coordinating to the lower Zn ion.

3.2. Double conformation and protonation state of GluB13 residues

T_6 insulin contains four glutamate residues (GluA4, GluA17, GluB13 and GluB21) per molecule. The pK_a value of independent glutamate is about 4.3. Since the crystal used in the neutron diffraction experiment was grown at pH 6.3, the glutamates should have been deprotonated from the viewpoint of a normal pK_a value. The results of the present neutron analysis indicated that GluA4, GluA17 and GluB21 had all been deprotonated (Table 2). However, the protonation state of GluB13 was found to be very complicated. This is of great interest because the carboxyl groups of the six GluB13 side chains form a compact core that is located in the centre of the insulin hexamer near the two Zn ions. The protonation or deprotonation of GluB13 is thus relevant to the local charge balance. If all GluB13 side chains were to be deprotonated, there would be six negative charges here, leaving a net charge of −2 after allowing for the two Zn^{2+} ions.

The side chains of GluB13 are frequently observed to be disordered in the $T_3R_3^f$ and R_6 hexamers; in the T_6 hexamer, however, disorder was observed for this residue for the first time in the structure of a dried crystal of T_6 human insulin at 100 K (Smith & Blessing, 2003).

A joint X-ray and neutron refinement experiment with T_6 porcine insulin (Wlodawer *et al.*, 1989) showed that the carboxylate O atoms of the two independent GluB13 side chains made a short contact of approximately 2.5 Å and that the carboxylate groups were suitably oriented for a hydrogen-bond interaction. However, since the crystal had been grown at a pH of approximately 6.5 and there was no evidence for a proton (or deuteron) in the neutron-density maps, the existence of a hydrogen bond could not be confirmed; instead, a nonbonded interaction was suggested. On the basis of biophysical chemical evidence that the isoionic point of GluB13 is 6.4 (Kaarsholm *et al.*, 1990) and the observation of a 2.46 Å contact between independent OE2 atoms in the 1.0 Å resolution structure of T_6 insulin at 120 K, Smith *et al.* (2003) suggested that a short strong centred carboxylate–carboxylic acid hydrogen bond linked the pairs of independent GluB13 carboxylate groups, with a proton shared about equally between the pairs of partially charged OE2 atoms.

In zinc-free cubic insulin the asymmetric unit contains a monomer and a crystallographic dyad generates the biologically relevant insulin dimer. Diao (2003) has shown that at pH < 5.80 GluB13 has a single conformation and that the carboxyl groups of GluB13 of two neighboring molecules interact with each other across a crystallographic dyad at a distance of 2.78 Å. This again suggests that one is protonated at pH < 5.80, allowing a hydrogen bond to form. At 6.00 < pH < 6.98 the GluB13 residue sometimes has two conformations and at high pH there is a complete switch to the second conformation, in which the carboxyl groups are further apart (Diao, 2003). In the neutron diffraction analysis of cubic porcine insulin at pD 6.6 (Ishikawa, Chatake, Ohnishi *et al.*, 2008) a double conformation of GluB13 was also observed and the occupancy of each conformation was set at 50%. The distance between the two carboxyl groups in the 'close-together' conformation was

Table 2
Protonation states of charged amino acids.

Circle, protonated; cross, deprotonated. D atoms of the N- and C-termini are represented by DN ter. and DC ter., respectively.

		Molecule 1	Molecule 2
GlyA1 N ter.	DN ter. 1	○	○
GlyA1 N ter.	DN ter. 2	○	○
GlyA1 N ter.	DN ter. 3	○	○
PheB1 N ter.	DN ter. 1	○	○
PheB1 N ter.	DN ter. 2	○	○
PheB1 N ter.	DN ter. 3	○	○
AsnA21 C ter.	DC ter.	×	×
AlaB30 C ter.	DC ter.	×	×
HisB5	DD1 (π)	○	○
HisB5	DE2 (τ)	○	○
HisB10	DD1 (π)	○	○
HisB10	DE2 (τ)	×	×
GluA4	DE2	×	×
GluA17	DE2	×	×
GluB13	DE2 (conformation I)	×	×
GluB13	DE2 (conformation II)	–	○
GluB21	DE2	×	×
ArgB22	DE	○	○
ArgB22	1DG1	○	○
ArgB22	2DG1	○	○
ArgB22	1DG2	○	○
ArgB22	2DG2	○	○
LysB29	DZ1	○	○
LysB29	DZ2	○	○
LysB29	DZ3	○	○

longer (3.1 Å) than in the X-ray results at pH < 5.80 (2.78 Å; Diao, 2003). (Note that Ishikawa and coworkers refer to the close-together conformation as conformation II, whereas Diao refers to it as conformation I; we use the nomenclature of Ishikawa and coworkers). Ishikawa, Chatake, Ohnishi *et al.* (2008) found that no proton could be identified between the two carboxyl groups and concluded that GluB13 was not protonated at pD 6.6. These results indicate that the chemical behaviour of the GluB13 carboxylate groups in dimeric insulin is similar to that observed in T_6 hexameric insulin.

In our neutron results on T_6 porcine insulin at pD 6.3 at room temperature, a double conformation of GluB13 was observed but only in molecule 2, as shown in Fig. 2. Moreover, since the resolution was higher than that of the joint X-ray and neutron refinement of T_6 porcine insulin (Wlodawer *et al.*, 1989), it was possible to observe that the OE2 atom of the GluB13.2 carboxylate group in conformation II was protonated. Therefore, the suggestion of Smith *et al.* (2003) was proven to be correct. In contrast, since the carboxyl groups of conformation I of the GluB13.2 side chain and of the GluB13.1 side chain were both deprotonated, a strong repulsion occurred between them. As a result, the GluB13.2 side chain in conformation I was forced to take a new position as shown in Fig. 2. We also considered the possibility of a double conformation of the carboxylate group of the GluB13.1 side chain, but refinement did not support a stable double conformation. On the contrary, the proton (DE2) of GluB13.2 in conformation II formed bifurcated hydrogen bonds to both the OE1 and OE2 atoms of GluB13.1. On refinement, the carboxylate group of the GluB13.1 side chain converged into a 90° rotated position which differs from that reported in the X-ray crystal structure analyses (Baker *et al.*, 1988; Wlodawer *et al.*, 1989; Smith *et al.*, 2003).

We also considered the possibility that the hydrogen bond between OE1 and OE2 (Fig. 2) might correspond to a low-barrier hydrogen bond (Cleland & Kreevoy, 1994; Frey *et al.*, 1994; Warshel *et al.*, 1995). However, the deviation of the D atom DE2 (1.0 Å) from the midpoint between OE1 and OE2 was 30% of the distance between OE1 and OE2 (3.3 Å), indicating that this was not a low-barrier hydrogen bond.

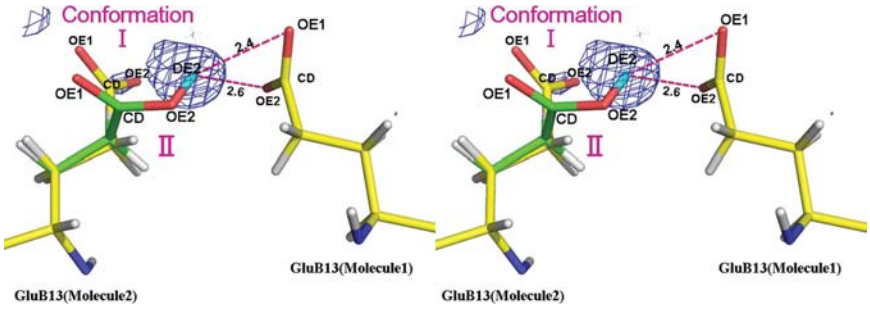

Figure 2
Stereoview of a $|F_o| - |F_c|$ positive nuclear density OMIT map of GluB13 (molecule 1) and GluB13 (molecule 2) contoured at 3σ, indicating the D atom between OE1 and OE2. The stereoview was prepared with the *PyMOL* program (DeLano, 2002).

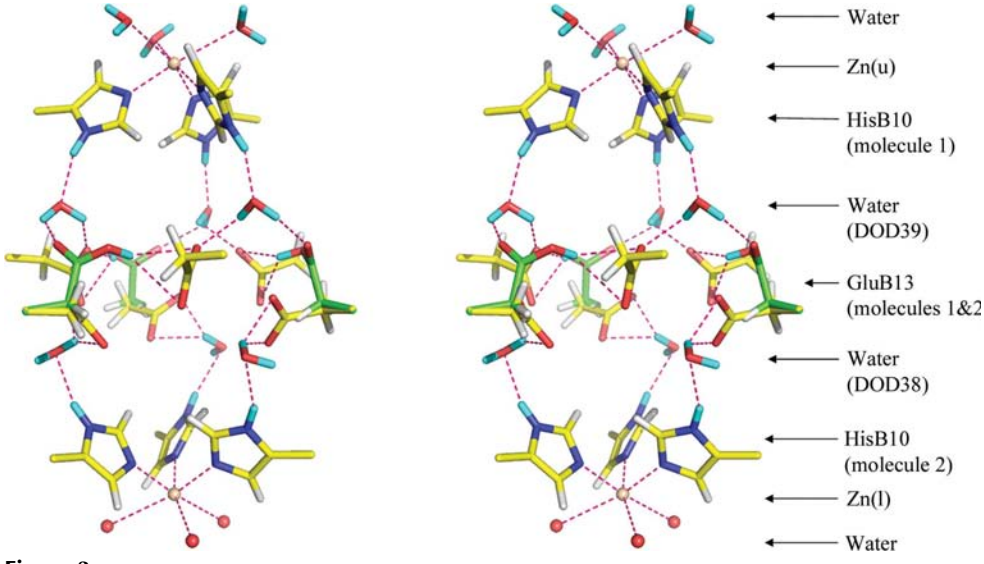

Figure 3
Stereoview of the hydrogen-bond network structure involving the GluB13 residues of molecules 1 and 2 between the two zinc ions that coordinate to the HisB10 residues. One side of the double conformation of GluB13 (molecule 2) is shown in green. The hydrogen-bond contacts of the water molecules are denoted by dotted lines. This stereoview was prepared with the *PyMOL* program (DeLano, 2002). (The detailed structure of GluB13 is shown in Fig. 4.)

3.3. Charge balance of zinc positive charges

The bivalent positive charge on the zinc should be balanced by separate but correlated negative ions (Baker *et al.*, 1988; Sakabe *et al.*, 1985). Here, it seems most probable that the positive charges of the zinc ions are balanced by negatively charged glutamic acid B13 carboxyl groups that lie in a layer midway between them. The HisB10.1 $N^{\delta1}$ atom is linked by a hydrogen-bonded water molecule to OE1 of GluB13 in molecule 2 of the dimer, as shown in Fig. 3, thus suggesting paths for charge transfer. The hydrogen-bond network indicated in Fig. 3 will be discussed in greater detail in §3.6.

Two zinc ions have four positive charges. If all the glutamic acid B13 residues (in the hexamer) were negatively charged (*i.e.* six negative charges), the proposed hexamer molecular arrangements would give two extra net negative charges. In our structure, a different possibility is suggested by the actual arrangement of the glutamate residues. The GluB13

cluster and the $(2F_o - F_c)$ positive nuclear density in our results at room temperature are illustrated in Fig. 4. Since the carboxyl group of GluB13 in molecule 1 was found to be deprotonated it had one negative charge; therefore, the net charge of GluB13 in molecule 1 was −3. On the other hand, it was also found that the side chain of GluB13 in molecule 2 had a double conformation in which one of the carboxyl groups of this double conformation was protonated but the other was deprotonated, as shown in Fig. 4. Thus, 50% of this carboxyl group had no charge and the other 50% had a negative charge; consequently, the net charge of GluB13 in molecule 2 was −3/2 and the net charge of GluB13 in the hexamer became −4.5 (= −3 − 3/2). Strictly speaking, the charge balance is still not completely fulfilled, but if we consider the accuracy of the occupancy of the double conformation, among other factors, the 0.5 charge difference might be within the acceptable error range.

The balance between the positive charge of the Zn ions and the negative charge of the GluB13 residues is thus explained by the identification of a proton bound to one of the carboxyl groups with double conformation.

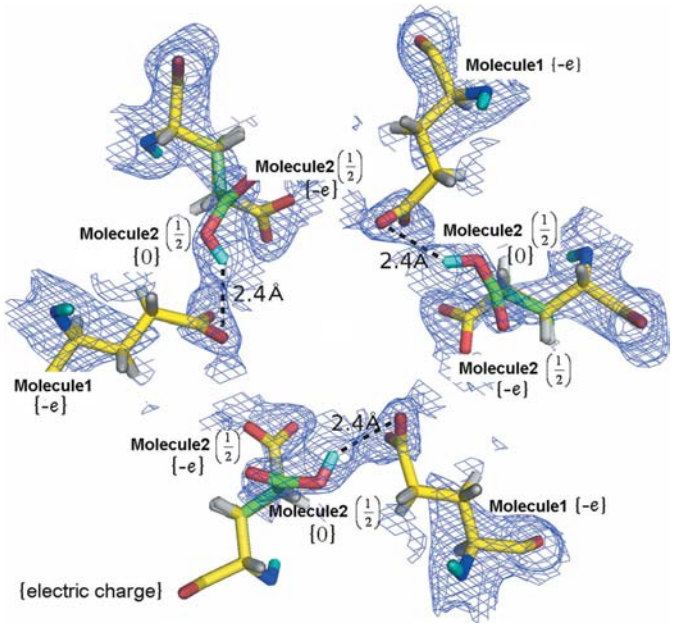

Figure 4
Charge distribution of the six GluB13 residues. The $2|F_o| - |F_c|$ positive nuclear density around the six GluB13 residues is shown contoured at 1σ. The half component of the double conformation of GluB13 in molecule 2, which was protonated, is shown in green; the proton is shown in cyan. Hydrogen-bond contacts are denoted by dotted lines. The electric charge of each GluB13 is shown in brackets. This figure was prepared with the *PyMOL* program (DeLano, 2002).

3.4. Comparison of histidines between T_6 insulin and cubic insulin

Insulin contains two histidines: HisB5 and HisB10. It was found that for HisB10 the $N^{\varepsilon 2}$ atoms were deprotonated and the $N^{\delta 1}$ atoms were protonated, whereas for HisB5 the $N^{\delta 1}$ and $N^{\varepsilon 2}$ atoms were both protonated. These results are expected if one considers that the $N^{\varepsilon 2}$ atoms of HisB10 coordinate the zinc ion and the $N^{\delta 1}$ atoms of HisB10 contribute to charge transfer between Zn and GluB13.

It is very interesting to compare the protonation and/or deprotonation states of HisB5 and HisB10 in the present T_6 insulin structure (which has the Zn-hexamer structure of the storage form) with those in cubic insulin (which belongs to an active form; Ishikawa, Chatake, Ohnishi *et al.*, 2008; Ishikawa, Chatake, Morimoto *et al.*, 2008). Neutron diffraction experiments on porcine cubic insulin (crystallized at pD values of 9.0 and 6.6) have already been performed by our group at room temperature (Ishikawa, Chatake, Morimoto *et al.*, 2008; Maeda *et al.*, 2004). We found that the pH-dependence of the protonation of HisB5 differed from that of HisB10. Both $N^{\delta 1}$ and $N^{\varepsilon 2}$ of HisB5 and HisB10 were protonated at pD 6.6. At pD 9.0 the $N^{\varepsilon 2}$ atom of HisB5 was not protonated; in fact, only the $N^{\delta 1}$ atom was protonated. However, both $N^{\varepsilon 2}$ and $N^{\delta 1}$ of HisB10 were again found to be protonated even at pD 9.0. These observations indicated that the pK_a value of HisB5 was normal but that the pK_a value of HisB10 was >9.0 and should be considered to be abnormal and indicative of a high affinity for positive ions. We infer that in the presence of Zn^{2+} ions the threefold symmetry-related $N^{\varepsilon 2}$ atoms of HisB10 coordinate to one Zn^{2+} ion and in the absence of Zn^{2+} ions HisB10 can capture a D^+ ion, thus guaranteeing the formation of the hexamer until Zn^{2+} ions are available (Ishikawa, Chatake, Morimoto *et al.*, 2008).

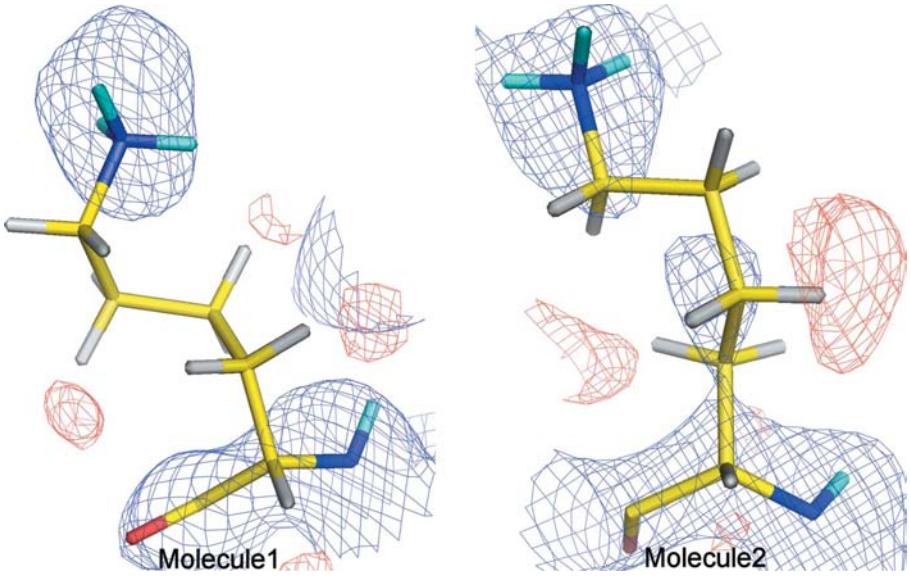

Figure 5
$2|F_o| - |F_c|$ positive nuclear density maps (blue, 1σ contours; red, -1.5σ contours) for LysB29 of molecules 1 and 2, respectively. This figure was prepared with the *PyMOL* program (DeLano, 2002).

Table 3
Hydrogen-bond distances and angles for GluB13.1 (conformation II), GluB13.2, HisB10.1 and HisB10.2.

Residue	Functional group	Donor/acceptor	Atom *X*	H	*Y*	Distance (Å)	Angle (°)
GluB13.1	COOH	Acceptor (◆)	GluB13.2 OE2	DE2	GluB13.1 OE1	2.44	140.5
		Acceptor (◆)	GluB13.2 OE2	DE3	GluB13.1 OE2	2.57	130.7
		Acceptor (◆)	DOD39 O	1D	GluB13.1 OE1	2.53	109.1
GluB13.2	COOH (I)	Acceptor (+)	DOD38 O	1D	GluB13.2 OE1	2.02	124.0
		Acceptor (+)	DOD38 O	1D	GluB13.2 OE2	2.28	138.6
		Acceptor (+)	DOD39# O	2D	GluB13.2 OE1	2.14	123.6
	COOH (II)	Donor (*)	GluB13.2 OE2	DE2	GluB13.1 OE1	2.44	140.5
		Donor (*)	GluB13.2 OE2	DE2	GluB13.1 OE2	2.57	130.7
HisB10.1	NH (aromatic)	Donor (■)	HisB10.1 ND1	DD1	DOD39 O	2.04	156.8
HisB10.2	NH (aromatic)	Donor (▲)	HisB10.2 ND1	DD1	DOD38 O	2.27	157.6

3.5. Protonation and deprotonation states of amino acids

The protonation states of the charged amino acids (Arg, Lys and Glu) were clearly observed; several distinctive features of each amino acid are discussed below and the results are completely summarized in Table 2.

Insulin has two N- and C-termini in each molecule because it consists of two chains. The average pK_a value of the α-NH_3^+ group was about 9.5 and that of the α-COO^- group was about 2.0. Therefore, at pD 6.3 the N-termini are expected to be protonated (NH_3^+) and the C-termini are expected to be deprotonated (COO^-). The results of our neutron study are consistent with these expectations and the results of our neutron-diffraction experiment have confirmed this.

Insulin has one lysine residue (B29) near the C-terminus of the B chain. The side chain of lysine is basic, with a pK_a of about 10.8; thus, at pD 6.3 lysine is expected to be protonated. Generally, in a medium-resolution neutron diffraction experiment the nuclear density of a CH_2 group is not observed because this group has a net neutron scattering length that is close to zero. However, an ND_3^+ group should be clearly observed because of its large neutron scattering length. This is the case in our structure, where the LysB29 residues in both molecules 1 and 2 are seen to be protonated as shown in Fig. 5.

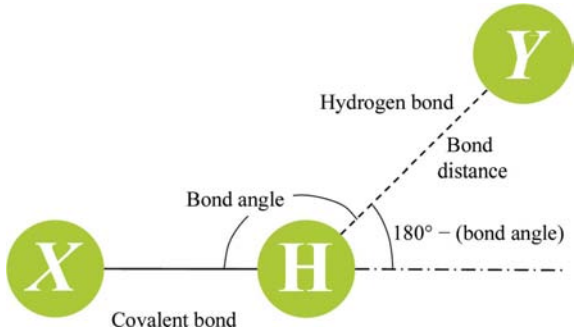

Figure 6
Geometric criteria for hydrogen bonds: *X* and *Y* are the hydrogen-bond donor and acceptor, respectively. In our analysis, the hydrogen-bond distances are defined by H···*Y* distances of less than 2.7, 2.6 and 3.1 Å for the acceptor atoms N, O and S, respectively; the hydrogen-bond angle is defined as the angle *X*—H···*Y*.

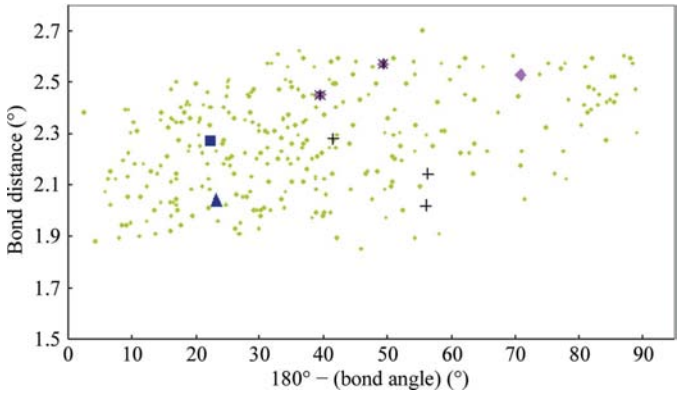

Figure 7
Distribution of hydrogen-bond distances and angles for acceptors (*Y*) in the T_6 insulin dimer in the present neutron analysis. Bond angles and distances are defined in Fig. 6. The symbols show the hydrogen bonds in the network structure, which consists of GluB13 through water molecules toward HisB10; the symbols correspond to those in Table 3. ◆, +, *, ■ and ▲ represent GluB13.1, GluB13.2 conformation I, GluB13.2 conformation II, HisB10.1 and HisB10.2, respectively.

3.6. Hydrogen bonds in T_6 insulin determined by neutron crystallography

Hydrogen bonds in the T_6 insulin dimer, as determined by the present neutron analysis, were identified using the following criteria. The hydrogen bond is defined as in Fig. 6, where *X*, *Y* and H are the donor, acceptor and H atom, respectively. Possible hydrogen bonds were inferred when the H···*Y* distances were less than 2.7, 2.6 and 3.1 Å for the acceptor atoms N, O and S, respectively. Hydrogen-bond angles were calculated as the supplementary *X*—H···*Y* angle (*i.e.* 180° minus the actual angle). Acceptor positions (*Y*) were searched, resulting in the identification of a total of 335 possible hydrogen bonds. The hydrogen-bond distances are plotted against hydrogen-bond angles in Fig. 7. Generally speaking, it is difficult to define the strength of a hydrogen bond, but as shown in Fig. 7 there is a tendency for there to be a weak but positive correlation between hydrogen-bond angle and distance (Baker & Hubbard, 1984).

The characteristics of the hydrogen bonds that form the network structure extending from GluB13 through water molecules toward HisB10 (Fig. 3) are summarized in Table 3; each hydrogen bond is denoted by a specific symbol in Fig. 7. The unique and important features of the hydrogen bonds involving GluB13 and HisB10 are interpreted as follows. Water molecules mediate the relationship between the HisB10 and GluB13 residues by forming rather strong hydrogen bonds. The hydrogen bonds between HisB10.1 (HisB10.2) and DOD39 (DOD38) appear to be strong because their hydrogen-bond lengths are short and the hydrogen-bond

angles are close to 180°. The hydrogen bonds between GluB13.2 and the water molecules are also strong, as deduced by their short bond lengths. In the central core-layer level, there are four hydrogen bonds between GluB13.1 and GluB13.2, and four hydrogen bonds between the water molecules and GluB13.1 (GluB13.2). The hydrogen bonds between GluB13.2 and GluB13.1, as shown in Fig. 2, are bifurcated. Although a single hydrogen bond alone is not very strong, the resultant strength of the bifurcated hydrogen bonds between them becomes rather strong because of the cooperation of the two hydrogen bonds. On the whole, the network structure consisting of GluB13 becomes very tight and stable.

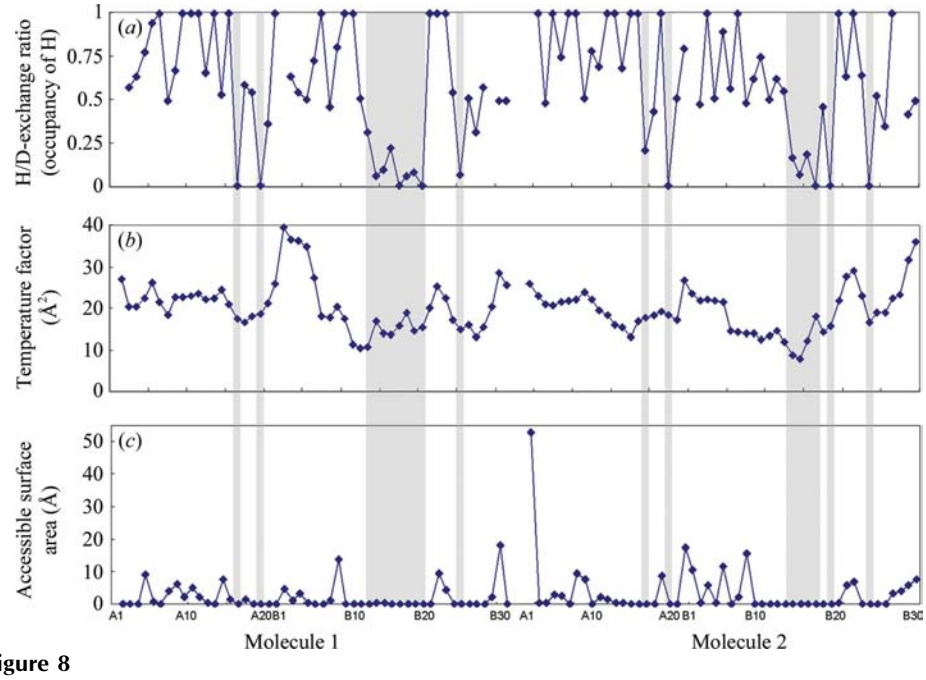

Figure 8
Hydrogen/deuterium (H/D) exchange ratios in T_6 insulin. (*a*) The H/D-exchange ratios, (*b*) the *B* factors and (*c*) the accessible surface areas (ASA) of the main-chain H/D atoms.

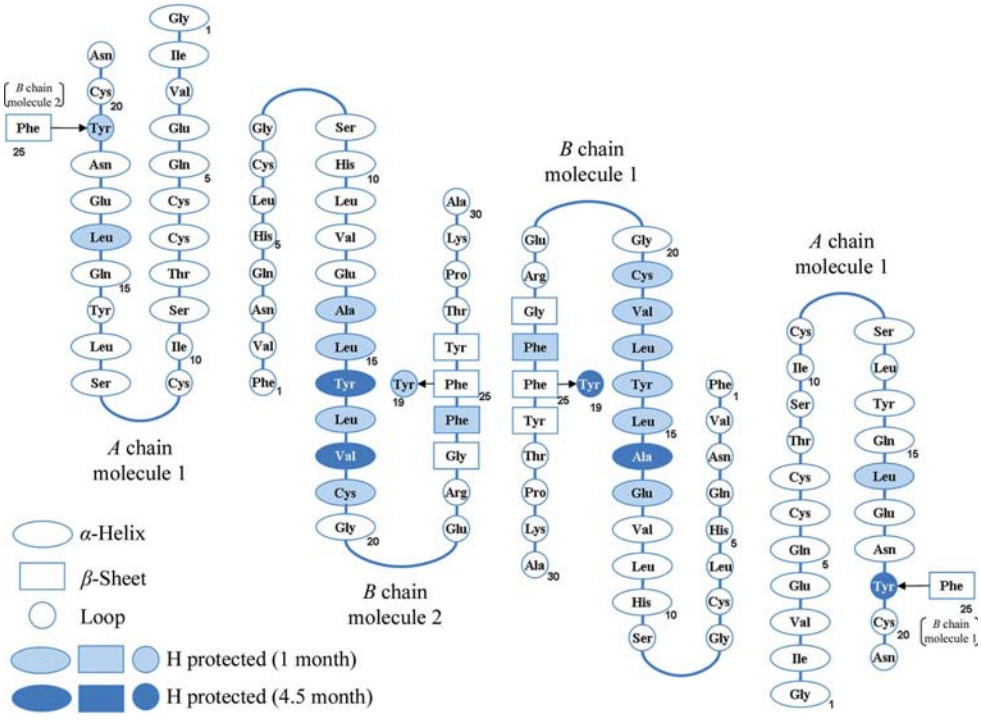

Figure 9
Diagram summarizing the time-evolution of the hydrogen/deuterium (H/D) exchange of amide H atoms (see §3.7). Here, the ellipses, rectangles and circles indicate amino acids belonging to α-helices, β-sheets and other regions (*e.g.* random loops), respectively. The open shapes indicate residues in which deuteration of the N—H groups is complete within one month, the shaded shapes indicate residues in which H/D exchange takes place in between one and 4.5 months and the filled shapes indicate residues in which N—H groups remain undeuterated even after 4.5 months of soaking the crystals in deuterated solution.

3.7. H/D exchange in T6 porcine insulin

The crystal used in our neutron-diffraction experiment was soaked in a deuterated solution for one month. As a result, the H/D-exchange ratios of the amide H atoms of T_6 porcine insulin in the crystals were obtained, as shown in Fig. 9(*a*). The error in the H/D-exchange ratio was assumed to be about 25%. There were 18 H atoms that were highly protected from H/D exchange and these were found to be concentrated in the centre of a helical region of the B chains.

Moreover, a correlation was found between the distribution of the *B* factors of the C^{α} atoms and the accessible surface area (ASA) of the main-chain atoms (probe radius = 1.4 Å). The 18 H/D atoms that had small H/D-exchange ratios also had small *B* factors and ASA values (Figs. 8*b* and 8*c*). These results not only indicate where those atoms are located in the interior of the protein molecule, but also suggest that the regions around those atoms have such a rigid structure that solvent molecules may be unable to contact them.

It is interesting to compare our results with those of Wlodawer *et al.* (1989) in discussing the H/D-exchange rate as a function of time. The D_2O-soaking periods of our crystals and those of

Wlodawer and coworkers were one month and 4.5 months, respectively. From the viewpoint of soaking time *versus* H/D-exchange ratios, we could classify the amide H atoms into three categories, as shown in Fig. 8: (i) those H atoms that were fully or partially deuterated after one month (shown as open symbols in Fig. 9), (ii) those in which H/D exchange occurred between one and 4.5 months (lightly shaded symbols in Fig. 9) and (iii) those in which amide H atoms were undeuterated (highly protected) even after 4.5 months (filled symbols in Fig. 9). The greatest protection of amide H atoms was in the centre of a helical region in each of the B chains (residues 14–19 in molecule 1 and 12–19 in molecule 2). This was in contrast to the observations in RNase A, in which amino-acid residues in β-sheets were more strongly protected from H/D exchange than those in α-helices (Wlodawer *et al.*, 1989). This indicates that H/D exchange in secondary structures depends on their location in the molecule. Moreover, it was found that the H/D-exchange rates for amide H atoms in the interior of the protein molecule were rather slow, *i.e.* of the order of a month.

4. Conclusion

A crystal structure of T_6 porcine insulin has been determined at the medium resolution of 2.1 Å using a BIX-4 single-crystal neutron diffractometer at the JRR-3 reactor of the Japan Atomic Energy Agency. The final values of the *R* factor and $R_{\rm free}$ were 17.9% and 25.6%, respectively, for 13 038 observed reflections and 4824 unique reflections with 89 water molecules. The following results were noted.

(i) Differences were observed in the dynamic behaviour of coordinated water molecules between the upper and lower Zn ions.

(ii) The double conformation of the GluB13 side chain in molecule 2 alone has been reconfirmed in the insulin hexamer.

(iii) The charge balance between Zn positive and GluB13 negative charges was reinterpreted in the light of the protonation and/or deprotonation states observed and their interaction among HisB10, water and GluB13.

(iv) The H/D-exchange ratios correlated with the *B* factors of the C^{α} atoms and the ASA values. Differences in the H/D-exchange ratios of the amide H atoms as a function of time (*i.e.* one month *versus* 4.5 month soak in D_2O) were measured and three different categories of H/D-exchange characteristics were classified.

(v) The hydrogen bonds in the network structure consisting of GluB13 through water molecules towards HisB10 are discussed in detail; it was found that the network structure was very tight and stable.

(vi) The abnormal pK_a value of HisB10 in cubic insulin was interpreted thus: the $N^{\varepsilon 2}$ atoms of HisB10 would eventually coordinate with Zn metal in the presence of Zn^{2+} ions.

We are grateful to Professor E. N. Baker for reading the manuscript and providing criticism and advice. This work was supported in part by a grant-in-aid for scientific research from the Ministry of Education, Culture, Sports, Science and Technology of Japan, from a Research Grant funded by the Human Frontier Science Program and a Collaborative Project between Ibaraki University, Hitachi Ltd and Ibaraki Prefecture.

References

Adams, M. J., Blundell, T. L., Dodson, E. J., Dodson, G. G., Vijayan, M., Baker, E. N., Harding, M. M., Hodgkin, D. C., Rimmer, B. & Sheat, S. (1969). *Nature (London)*, **224**, 491–495.
Baker, E. N., Blundell, T. L., Cutfield, J. F., Cutfield, S. M., Dodson, E. J., Dodson, G. G., Hodgkin, D. C., Hubbard, R. E., Isaacs, N. W., Reynolds, C. D., Sakabe, K., Sakabe, N. & Vijayan, N. M. (1988). *Philos. Trans. R. Soc. London Ser. B*, **319**, 369–456.
Baker, E. N. & Hubbard, R. E. (1984). *Prog. Biophys. Mol. Biol.* **44**, 97–179.
Blundell, T. L., Dodson, G. G., Dodson, E. J., Hodgkin, D. C. & Vijayan, M. (1971). *Recent Prog. Horm. Res.* **27**, 1–40.
Blundell, T. L., Dodson, G. G., Hodgkin, D. C. & Mercola, D. A. (1972). *Adv. Protein Chem.* **26**, 279–402.
Brünger, A. T. (1992). *Nature (London)*, **355**, 472–474.
Brünger, A. T., Adams, P. D., Clore, G. M., DeLano, W. L., Gros, P., Grosse-Kunstleve, R. W., Jiang, J.-S., Kuszewski, J., Nilges, M., Pannu, N. S., Read, R. J., Rice, L. M., Simonson, T. & Warren, G. L. (1998). *Acta Cryst.* D**54**, 905–921.
Brzovic, P. S., Choi, W. E., Borchardt, D., Kaarsholm, N. C. & Dunn, M. F. (1994). *Biochemistry*, **33**, 13057–13069.
Chatake, T., Ostermann, A., Kurihara, K., Parak, F. G. & Niimura, N. (2003). *Proteins*, **50**, 516–523.
Cleland, W. W. & Kreevoy, M. M. (1994). *Science*, **264**, 1887–1890.
Collaborative Computational Project, Number 4 (1994). *Acta Cryst.* D**50**, 760–763.
DeLano, W. L. (2002). *The PyMOL Molecular Graphics System.* DeLano Scientific LLC, San Carlos, California, USA. http://www.pymol.org.
Diao, J. (2003). *Acta Cryst.* D**59**, 670–676.
Frey, P. A., Whitt, S. A. & Tobin, J. B. (1994). *Science*, **264**, 1927–1930.
Goldman, J. & Carpenter, F. H. (1974). *Biochemistry*, **13**, 4566–4574.
Ishikawa, T., Chatake, T., Morimoto, Y., Maeda, M., Kurihara, K., Tanaka, I. & Niimura, N. (2008). *Biochem. Biophys. Res. Commun.* **376**, 32–35.
Ishikawa, T., Chatake, T., Ohnishi, Y., Tanaka, I., Kurihara, K., Kuroki, R. & Niimura, N. (2008). *Chem. Phys.* **345**, 152–158.
Kaarsholm, N. C., Havelund, S. & Hougaard, P. (1990). *Arch. Biochem. Biophys.* **283**, 496–502.
Kurihara, K., Tanaka, I., Refai Muslih, M., Ostermann, A. & Niimura, N. (2004). *J. Synchrotron Rad.* **11**, 68–71.
Maeda, M., Chatake, T., Tanaka, I., Ostermann, A. & Niimura, N. (2004). *J. Synchrotron Rad.* **11**, 41–44.
McRee, C. E. (1999). *J. Struct. Biol.* **125**, 156–165.
Niimura, N., Arai, S., Kurihara, K., Chatake, T., Tanaka, I. & Bau, R. (2006). *Cell. Mol. Life Sci.* **63**, 285–300.
Niimura, N., Karasawa, Y., Tanaka, I., Miyahara, J., Akahashi, K., Saito, H., Koizumi, S. & Hidaka, M. (1994). *Nucl. Instrum. Methods A*, **349**, 521–525.
Ohnishi, Y., Yamada, T., Tanaka, I. & Niimura, N. (2009). In preparation.
Otwinowski, Z. & Minor, W. (1997). *Methods Enzymol.* **276**, 307–326.
Sakabe, N., Sakabe, K. & Sasaki, K. (1985). *J. Biosci.* **8**, 45–55.
Smith, G. D. & Blessing, R. H. (2003). *Acta Cryst.* D**59**, 1384–1394.
Smith, G. D., Pangborn, W. A. & Blessing, R. H. (2003). *Acta Cryst.* D**59**, 474–482.
Swanson, S. M. (1988). *Acta Cryst.* A**44**, 437–442.
Warshel, A., Papazyan, A. & Kollman, P. (1995). *Science*, **269**, 102–106.
Wlodawer, A., Savage, H. & Dodson, G. (1989). *Acta Cryst.* B**45**, 99–107.